Influence of physical perturbation on Fe(II) supply in coastal marine sediments

Ulf Lueder[1], Markus Maisch[1], Katja Laufer[2,3], Bo Barker Jørgensen[2], Andreas Kappler[1,2], Caroline Schmidt[1*]

[1] Geomicrobiology Group, Center for Applied Geoscience (ZAG), University of Tuebingen, Sigwartstrasse 10, D-72076 Tuebingen, Germany

[2] Center for Geomicrobiology, Department of Bioscience, Aarhus University, Ny Munkegade 114, Building 1540, 8000 Aarhus, Denmark

[3] GEOMAR Helmholtz Center for Ocean Research Kiel, Wischhofstraße 1-3 24148 Kiel, Germany

Supporting Information

Number of tables in supporting information: 1

Number of figures in supporting information: 12

Total numbers of pages in supporting information: 13 (including cover page)

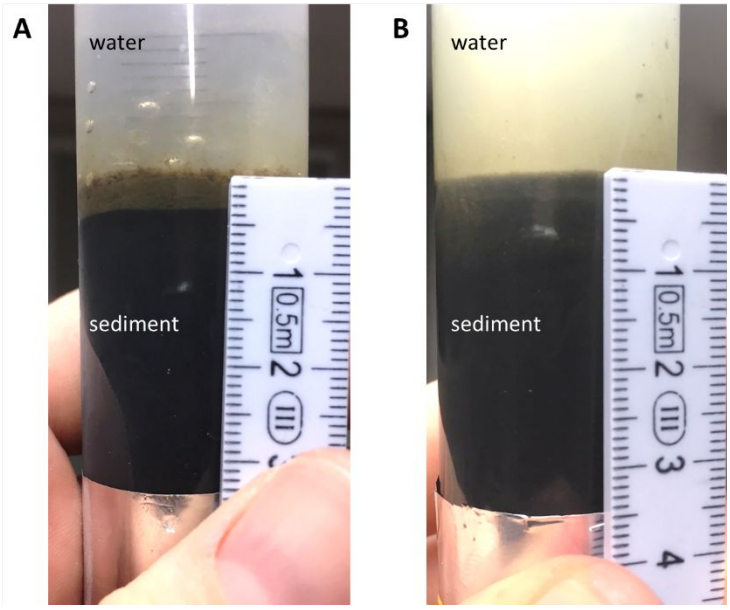

Figure S1. One of the 17 sediment cores prepared for this study from homogenized sediment in order to enable reproducible starting conditions of the sediment cores, (A) after 7 days of undisturbed 12 h light-dark incubation, (B) shortly after the simulated storm event. Please note the difference in turbidity due to suspended sediment after the storm event.

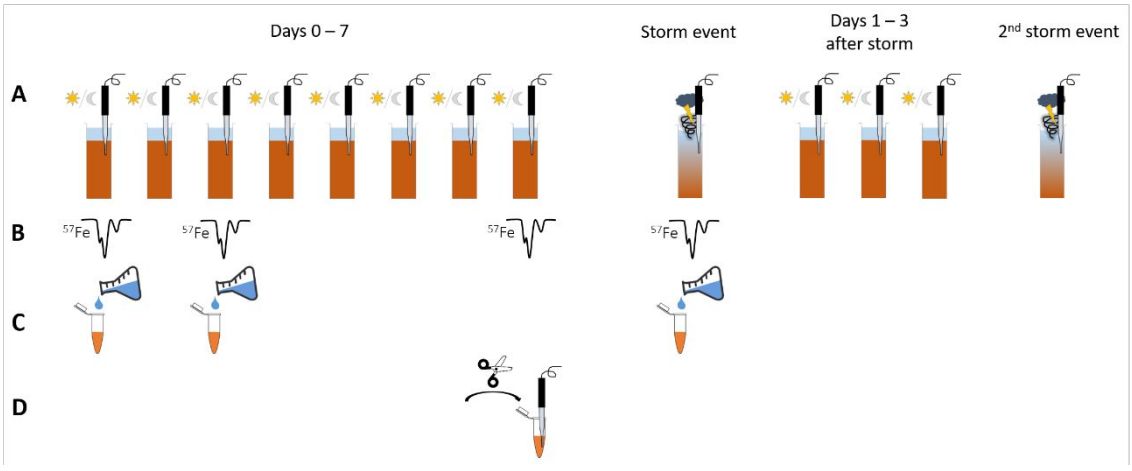

Figure S2. Scheme of the experimental approach, (A) Daily microsensor measurements during undisturbed 12 h light-dark incubation and shortly after storm events, (B) selected time points for Mössbauer spectroscopy analysis, (C) selected time points for sequential Fe extractions and (D) test of the impact of physical perturbation simply due to slicing the sediment core and voltammetric measurements in the sediment slurry and centrifuged supernatant.

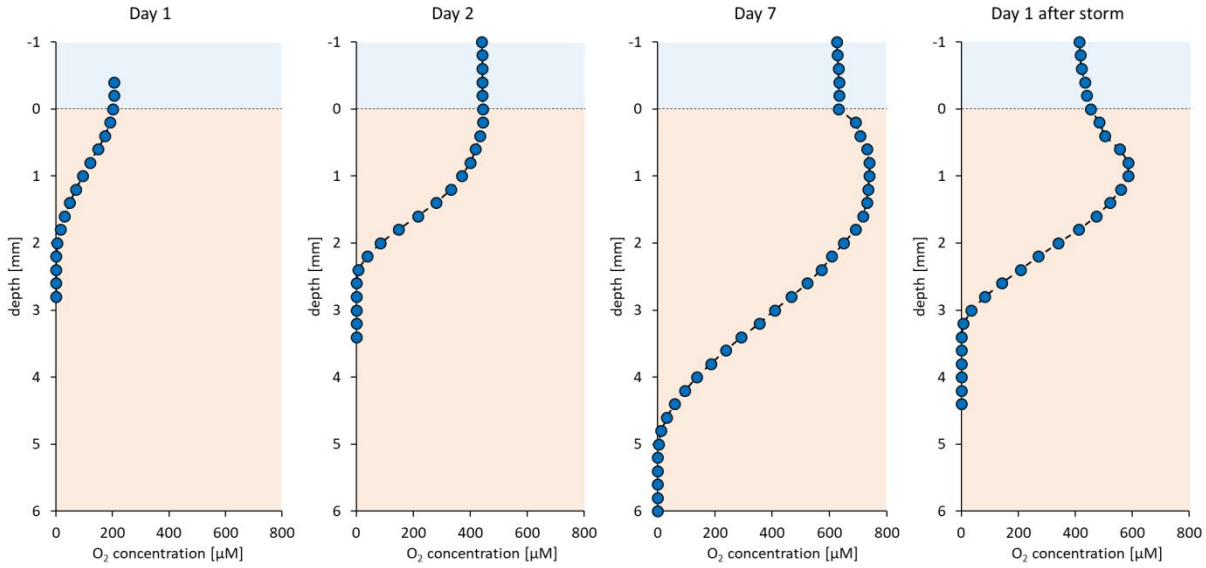

Figure S3. O_2 concentration profiles after 1, 2 and 7 days of undisturbed 12h light-dark incubation and 1 day after the simulated storm event.

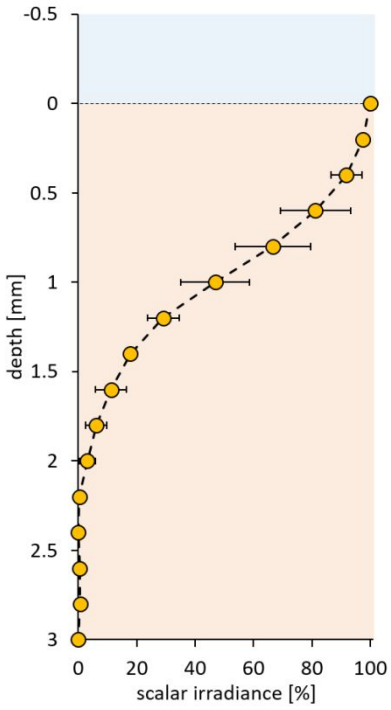

Figure S4. Light intensity (expressed as scalar irradiance) in the sediment, normalized to the light intensity reaching the sediment surface. Error bars show the standard deviation of five recorded scalar irradiance profiles.

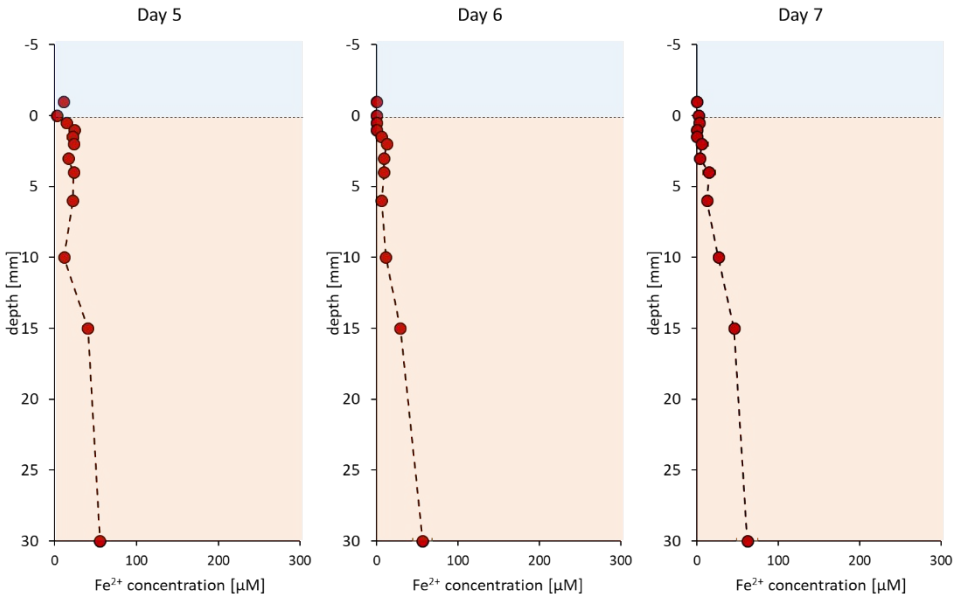

Figure S5. Fe^{2+} concentration profiles after 5, 6 and 7 days of undisturbed 12h light-dark incubation.

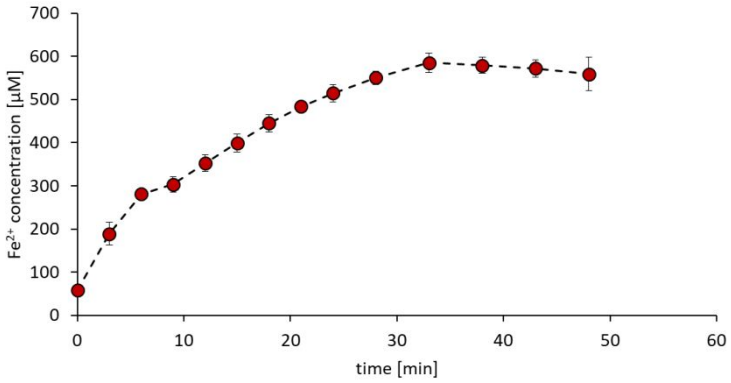

Figure S6. Fe^{2+} development during a simulated storm event in the sediment core determined by voltammetric measurements. The high Fe^{2+} concentrations reaching >500 µM can be attributed to release of Fe^{2+}, e.g. from metastable FeS_x mineral phases into the sedimentary pore water during the physical perturbation without subsequent equilibration of the sediment. Error bars show standard deviation of triplicate voltammograms.

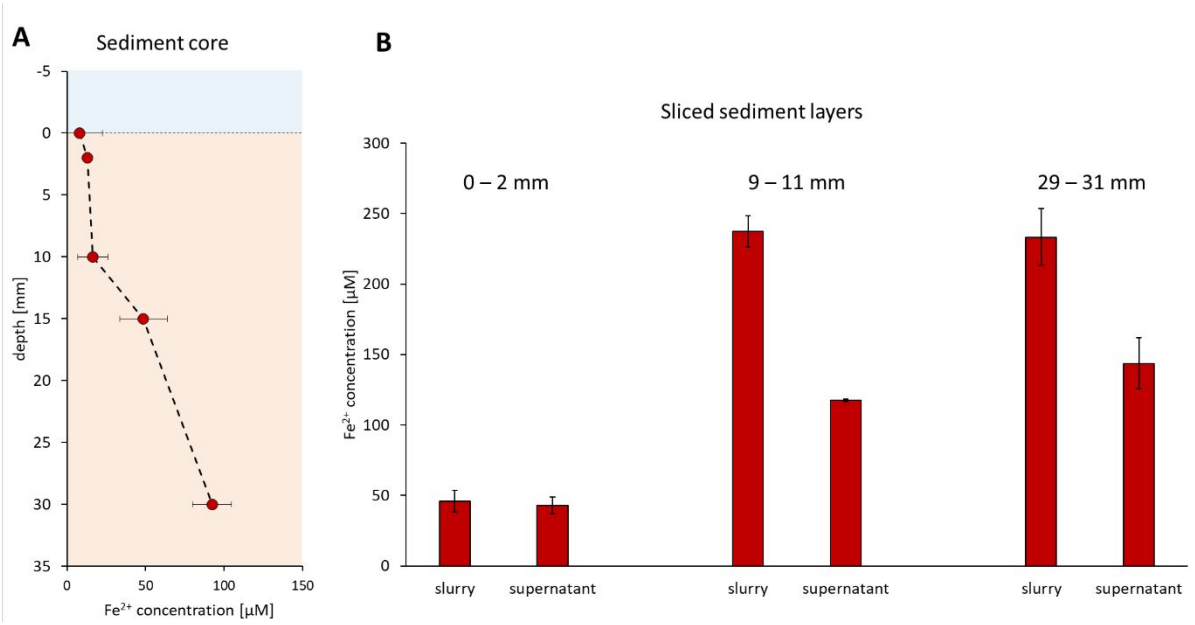

Figure S7. Impact of physical movement (slicing and homogenization) of sediment on Fe^{2+} mobilization, (A) Fe^{2+} concentrations in an undisturbed sediment core determined by voltammetry, (B) Fe^{2+} concentrations in sliced and homogenized sediment layers (0-2 mm, 9-11 mm and 29-31 mm depth) determined in the homogenized sediment slurry and in the supernatant of centrifuged sediment. Error bars show standard deviation of triplicate voltammograms.

Cyclone Christian with wind speeds of up to 190 km h^{-1} did hit western Europe in October 2013. During this storm, the water and sediment of the sampling site Norsminde Fjord (Denmark) were completely mixed and resuspended. Microsensor profiles of O_2 and redox potential were recorded in in-situ sediment cores before and 2 days after this storm event (Figure S7).

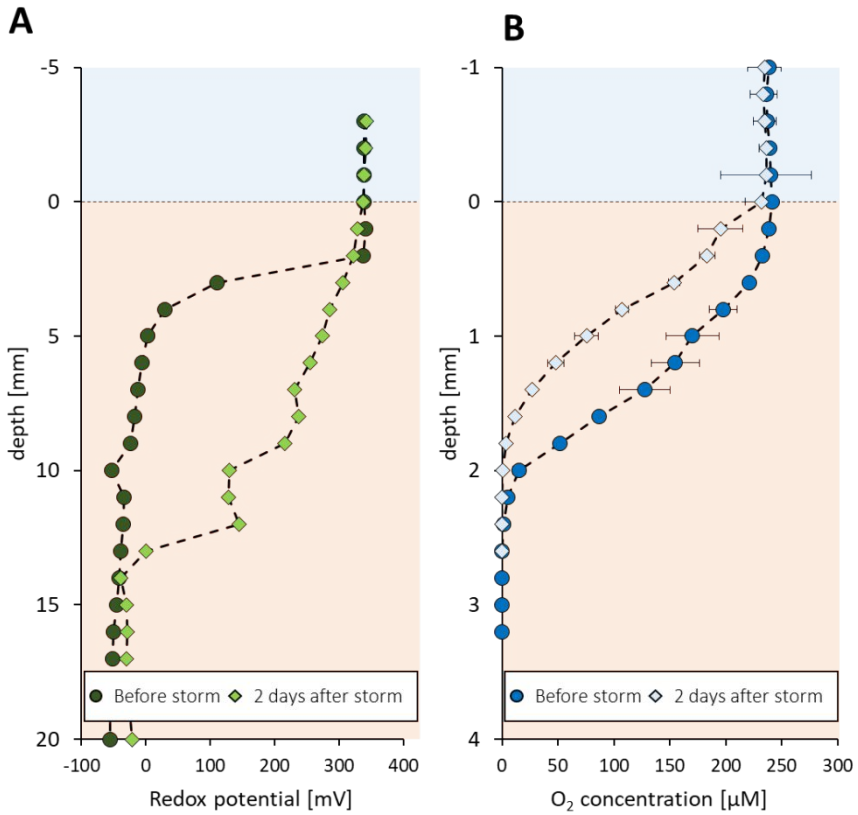

Figure S8. Profiles in in-situ sediment cores before and 2 days after a storm at the sampling field site, (A) redox potential profiles, (B) O_2 concentration profiles. Error bars show the standard deviation of triplicate measurements. Note the different scales of the y-axes.

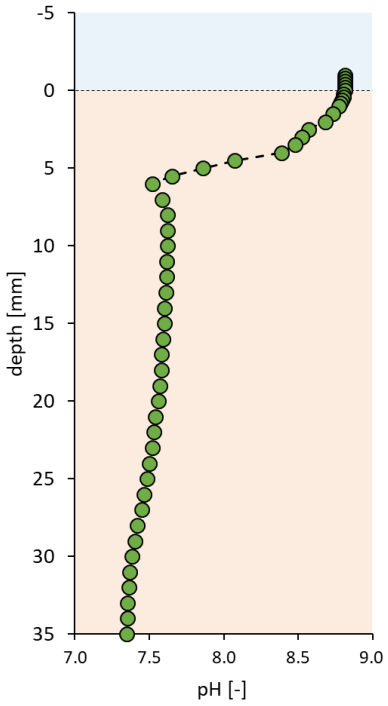

Figure S9. pH profile recorded before the 2nd simulated storm event. Oxygenic photosynthesis in the oxic sediment layers lead to elevated pH values.

Mössbauer spectroscopy & XRD data

Mössbauer spectroscopy parameters are listed in Table S1. The spectra collected at 77 K show two clear and well pronounced doublet features (Db), with one broad doublet (Db1) and a narrow doublet (Db2) which are overlapping at the isomer center (Figure S9). The hyperfine parameters of these two doublets have very similar properties for all four samples at 77 K with a center shift (CS) of CS = 1.23 – 1.25 mm s^{-1} for Db1 and CS = 0.42 mm s^{-1} for Db2. The relatively high quadrupole splitting (ΔE_Q) of ΔE_Q = 2.9 mm s^{-1} for Db1 is suggesting the presence of a high spin Fe(II) mineral phase with a relative abundance of around 40.5 ± 1.5% in all samples. The low quadrupole splitting parameters of Db2 with ΔE_Q = 0.57 ± 0.1 mm s^{-1} could be interpreted as high-spin Fe(III) phase or low-spin Fe(II). In order to resolve this uncertainty, the sample was additionally analyzed at 5 K. The narrow splitting which resulted at the low temperature confirmed the absence of an internal field and a magnetic ordering and implies the presence of a second Fe(II) phase – a low-spin Fe(II) mineral. Spectra that were

collected at 5 K show a high similarity to spectra collected at 77 K. The wide Db1 and narrow Db2 are the predominant features in all samples. Their hyperfine characteristics change slightly with a decrease in their center shift to CS = 1.13 ± 0.05 mm s^{-1} for Db1 and CS = 0.41 ± 0.01 mm s^{-1} for Db2. The increase in their quadrupole splitting to ΔE_Q = 2.9 ± 0.2 mm s^{-1} for Db1 and ΔE_Q = 0.67 ± 0.3 mm s^{-1} for Db2 is consistent with their interpretation as a high-spin Fe(II) phase represented by Db1 and an additional low-spin Fe(II) phase being detected in Db2. In addition to the doublet features, also the presence of a magnetically-ordered iron phase can be interpreted by the residual peaks in the background. In order to achieve a satisfactory fit, an additional poorly defined hyperfine field distribution site (HFD-site) with two components was required. The best-fit model for all spectra collected at 5 K (Figure S10) suggests a narrow sextet (S1), composing of two fitting components with relatively consistent hyperfine field parameters, CS at around CS = 0.45 – 0.9 mm s^{-1} and a hyperfine field (B_{hf}) of B_{hf} = 23 – 27 T. According to Wan et al. [1] and Thiel et al.[2], this poorly defined sextet could potentially resemble a metastable iron-sulphur mineral phase (FeS_x) undergoing magnetic ordering at 5 K that is present in all samples. The magnetic resonance splitting of this metastable mineral phase was potentially hidden behind the well pronounced doublet features of Db1 and Db2 at the higher temperature of 77 K but only became detectable at 5 K. The hyperfine field parameters of Db2 do not allow a clear identification of one specific ferrous iron mineral compound. However, the absence of a magnetic ordering at low temperature and the resulting fitting parameters indicate that a high-spin Fe(II) phase is being represented herein, with vivianite, siderite and melanterite as most potential candidates.[3] Hyperfine field parameters of the narrow doublet Db2 are very similar to pyrite (FeS_2) as a low-spin Fe(II) phase. As stated above, the relative abundance of these two mineral phases is relatively consistent among the 77 K spectra (Table S1) with FeS_2 being the more dominant phase over potential Fe(II) (oxyhydr)oxides. However, considering the fit-model of the 5 K spectra, the relative abundances of all three iron phases vary slightly.

Table S1. Hyperfine parameters: Sample name, temperature sample was analyzed at, CS – Center shift, ΔE_Q – Quadrupole splitting, ε – Quadrupole shift, B_{hf} – Hyperfine field, Pop. – relative abundance, χ^2 – goodness of fit, matched candidate phase with $Fe(II)_{ppt}$ = Fe(II) (oxyhydr)oxide.

Sample	Temp. [K]	Phase	CS [mm s^{-1}]	ΔE_Q [mm s^{-1}]	ε [mm s^{-1}]	B_{hf} [T]	Pop [%]	±	χ^2	Mineral phase
Day 0	77	Db1	1.25	2.91			41.8	0.3	0.57	$Fe(II)_{ppt}$
		Db2	0.44	0.56			58.2	0.2		Pyrite
	5	Db1	1.13	2.88			40.6	1.1	0.72	$Fe(II)_{ppt}$
		Db2	0.40	0.66			39.0	0.3		Pyrite
		S1	0.54		0.08	28.7	20.4	2.9		FeS_x
Day 2	77	Db1	1.25	2.93			41.6	0.2	0.62	$Fe(II)_{ppt}$
		Db2	0.44	0.57			58.4	0.2		Pyrite
	5	Db1	1.19	2.99			28.7	0.3	0.84	$Fe(II)_{ppt}$
		Db2	0.42	0.65			49.1	0.4		Pyrite
		S1	0.87		0.12	23.7	232	1.36		FeS_x
Day 7	77	Db1	1.24	2.92			40.5	0.3	0.68	$Fe(II)_{ppt}$
		Db2	0.44	0.60			59.5			Pyrite
	5	Db1	1.17	3.10			31.3	0.4	0.79	$Fe(II)_{ppt}$
		Db2	0.41	0.69			45.0	0.3		Pyrite
		S1	0.98		-0.04	27.0	23.7	1.9		FeS_x
After storm	77	Db1	1.23	2.94			38.7	0.3	0.79	$Fe(II)_{ppt}$
		Db2	0.42	0.58			61.3	0.2		Pyrite
	5	Db1	1.02	2.84			46.1	1.9	0.98	$Fe(II)_{ppt}$
		Db2	0.40	0.63			35.9	0.6		Pyrite
		S1	0.44		0.03	27.6	18.0	1.3		FeS_x

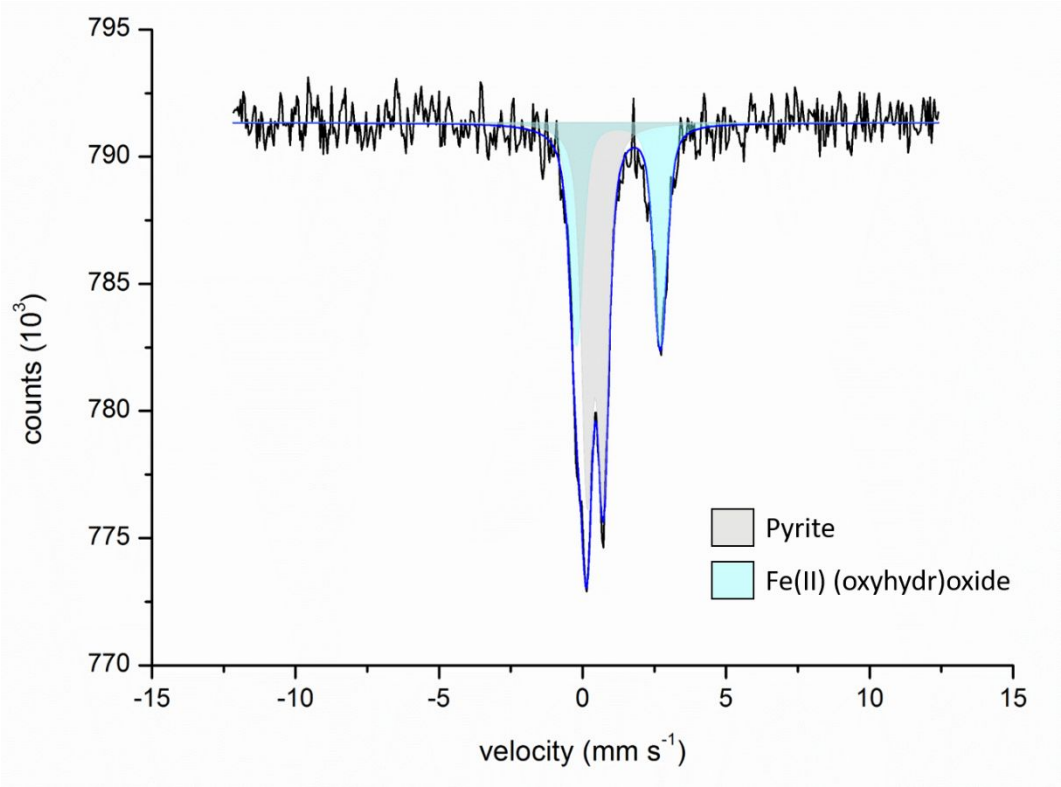

Figure S10. Representative Mössbauer model fit (blue line) of spectra collected at 77 K (black line), characterized by two dominant doublets, likely representing a high-spin Fe(II) (oxyhydr)oxide (light blue) and pyrite (grey).

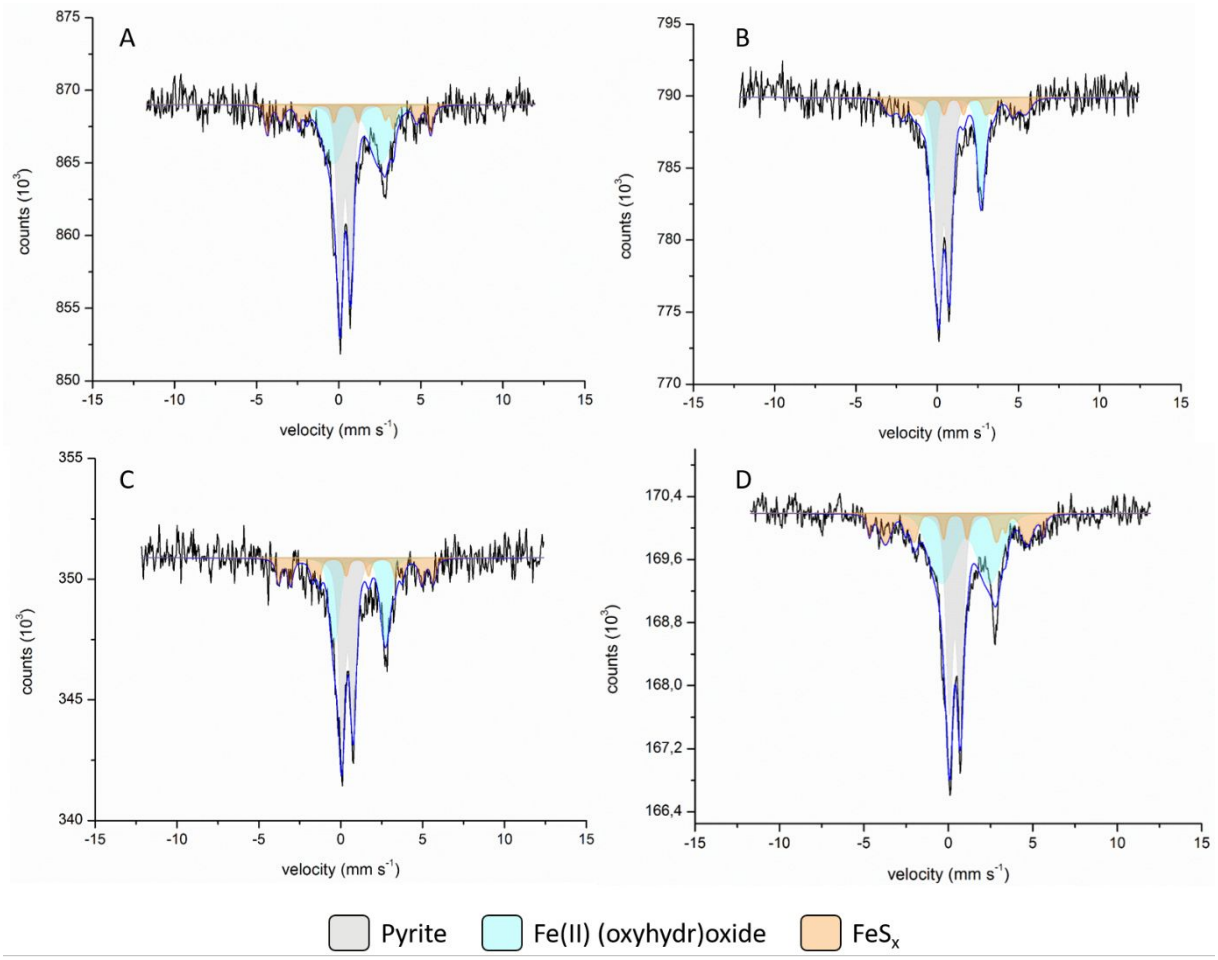

Figure S11. Mössbauer spectroscopy – Model fit (blue line) of spectra collected at 5 K (black line) for samples of (A) day 0, (B) day 2 and (C) day 7 of undisturbed light-dark incubation as well as (D) after the simulated storm event. All samples show two dominant doublet features that can likely be attributed to the presence of a high-spin Fe(II) (oxyhydr)oxide (light blue), pyrite (grey) and a poorly developed sextet potentially representing a metastable Fe-S-phase (FeS_x, orange).

The sediment sample for an identification by XRD was collected and dried under anoxic conditions, loaded onto a silica wafer (sample size ø 2mm) and kept constantly anoxic until analysis. The analysis was carried out on a 2D-Microdiffractometer (Bruker D8 Discover with GADDS, μ-XRD², Bruker AXS GmbH, Karlsruhe, Germany), using a cobalt anode tube as x-ray source with a Co-Kα wavelength of 1.79030 Å and a 2D detector with 40° angle cover (Bruker Våntec 500 Bruker AXS GmbH, Karlsruhe, Germany). The sample was not rotated and reflection patterns were collected for 120 seconds per angle setting. Reflection pattern analysis and mineral identification was carried out using Match! program for phase identification from powder diffraction (Match!, Crystal Impact, Bonn, Germany). XRD diffraction pattern of both samples, wet and dried sediment, showed a clear signal for quartz

being the most dominant and crystalline mineral phase in the sediment matrix (Figure S11). In the wet sample, small reflections were detected that could be indicative for FeS_2 being present as Fe(II) mineral. However, the reflections were not significant enough to clearly confirm its presence, potentially due to scattering interferences with the wet sample matrix. As FeS_2 is thermodynamically more stable than Fe monosulphides [4] and the oxidation kinetics of FeS_2 by O_2 is significantly slower after the formation and accumulation of a ferric oxyhydroxide layer on the sulphide surface [5], the sample was dried in air for some minutes in order to remove the water from the sediment matrix. The XRD pattern of the dried sample showed the two major reflections for FeS_2 and clearly approved its presence as Fe(II) phase. Due to the drying process, also halite (NaCl) crystallized and precipitated as an evaporation product (Figure S11).

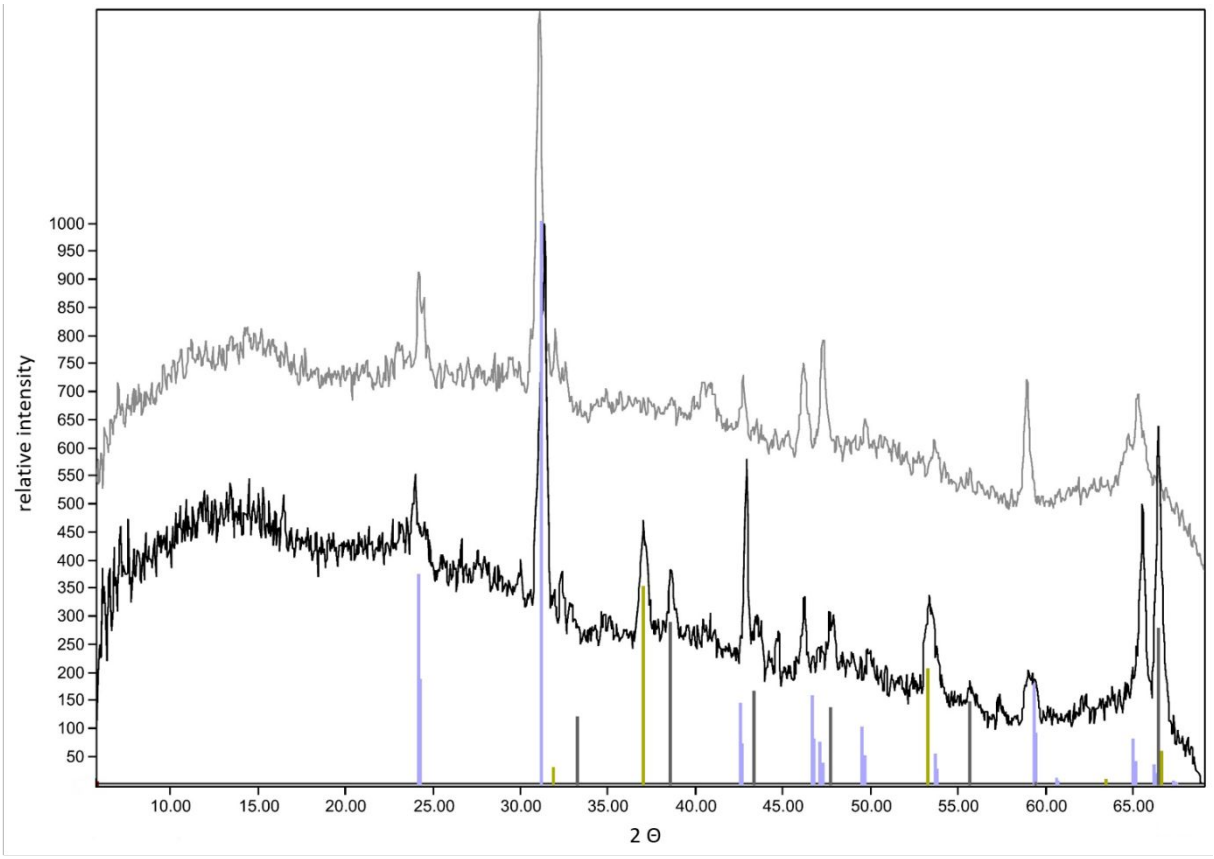

Figure S12. X-ray diffraction pattern collected from the native sample material (anoxic, wet – upper, grey line) and the dried sediment material (air-dried – lower, black line). Both patterns show a clear signal for quartz (light blue reference). FeS_2 (grey reference) was clearly detectable in the air-dried sample material only, while also halite (NaCl – olive reference) precipitated in the air-dried sediment due to evaporation.

References

1. Wan, M.; Schröder, C.; Peiffer, S., Fe(III):S(-II) concentration ratio controls the pathway and the kinetics of pyrite formation during sulfidation of ferric hydroxides. *Geochim. Cosmochim. Acta* **2017,** *217*, 334-348.
2. Thiel, J.; Byrne, J.; Kappler, A.; Schink, B.; Pester, M., Pyrite formation from FeS and H_2S is mediated by a novel type of microbial energy metabolism. *bioRxiv* **2018**, 396978.
3. Taneja, S. P.; Jones, C. H. W., Mossbauer Studies of Iron-Bearing Minerals in Coal and Coal Ash. *Fuel* **1984,** *63*, (5), 695-701.
4. Giblin, A. E.; Howarth, R. W., Porewater evidence for a dynamic sedimentary iron cycle in salt marshes1. *Limnol. Oceanogr.* **1984,** *29*, (1), 47-63.
5. Nicholson, R. V.; Gillham, R. W.; Reardon, E. J., Pyrite oxidation in carbonate-buffered solution: 2. Rate control by oxide coatings. *Geochim. Cosmochim. Acta* **1990,** *54*, (2), 395-402.